Smart Structures and Systems, *Vol. 19, No. 6 (2017) 633-641*
DOI: https://doi.org/10.12989/sss.2017.19.6.633

Modeling techniques for active shape and vibration control of macro-fiber composite laminated structures

Shun-Qi Zhang[1,3a], Min Chen[4b], Guo-Zhong Zhao[3c],
Zhan-Xi Wang[*2], Rüdiger Schmidt[5d] and Xian-Sheng Qin[2e]

[1]School of Mechatronic Engineering and Automation, Shanghai University, Shanghai 200444, P.R. China
[2]School of Mechanical Engineering, Northwestern Polytechnical University, Xi'an 710072, P.R. China
[3]State Key Laboratory of Structural Analysis for Industrial Equipment, Dalian University of Technology, Dalian 116024, P.R. China
[4]Department of Industrial Design, Xi'an Jiaotong - Liverpool University, Suzhou 215123, P.R. China
[5]Institute of Structural Mechanics and Lightweight Design, RWTH Aachen University, Aachen 52062, Germany

(Received September 26, 2016, Revised November 17, 2016, Accepted March 12, 2017)

Abstract. The complexity of macro-fiber composite (MFC) materials increasing the difficulty in simulation and analysis of MFC integrated structures. To give an accurate prediction of MFC bonded smart structures for the simulation of shape and vibration control, the paper develops a linear electro-mechanically coupled static and dynamic finite element (FE) models based on the first-order shear deformation (FOSD) hypothesis. Two different types of MFCs are modeled and analyzed, namely MFC-d31 and MFC-d33, in which the former one is dominated by the d_{31} effect, while the latter one by the d_{33} effect. The present model is first applied to an MFC-d33 bonded composite plate, and then is used to analyze both active shape and vibration control for MFC-d31/-d33 bonded plate with various piezoelectric fiber orientations.

Keywords: macro-fiber composite; smart structures; dynamic analysis; piezoelectric; laminated structures

1. Introduction

Structures bonded with piezoelectric materials, called 'smart structures', have a great potential in the application of shape control, vibration suppression, health monitoring (Konka *et al*. 2013) and energy harvesting (Song *et al*. 2010), especially for plate and shell structures in aerospace engineering. In the past three decades a lot of research has been published concerning conventional piezoceramics or piezopolymers. It can be found that piezoceramics, like lead zirconium titanate (PZT), have relatively strong actuation forces, but the brittle nature of ceramics makes them being easily damaged during handling and bonding processes (Williams *et al.* 2002a). Piezoelectric polymers, like polyvinylidene fluoride (PVDF), are much more flexible, but with lower actuation forces compared to PZT.

To overcome these limitations of piezoelectric materials, piezo composite materials were developed and introduced to industries. The first type of piezo composite is referred to 1-3 composites invented by Skinner *et al.* (1978), the second one is an active fiber composite (AFC) initially developed by MIT (Hagood *et al.* 1993, Bent and Hagood 1997) and the third one is a macro-fiber composite (MFC) proposed by NASA Langley Research Center (Wilkie *et al*. 2000). For more details of piezo composites, the paper refers to the references (Williams *et al*. 2002b, Lin *et al*. 2013). The structural mechanism of AFC and MFC patches are quite similar. The major difference is that AFC patches include circular cross-section piezoelectric fibers, while MFC patches use rectangular cross-section fibers. Due to circular cross-section piezoelectric fibers in AFC, the contact area between the interdigitated electrodes and the fibers is so small that it needs high operating voltage (Park and Kim 2005). Therefore, among all these piezoelectric composite materials, the MFC is the leading low-profile actuator and sensor offering high performance, flexibility and reliability in a cost competitive device (Smart Material Corp. 2016). MFC is comprised of an active layer in the middle, electrode layers and kapton protection films. The active layer is constructed by piezoceramic fibrous phase embedded in epoxy matrix. This kind of structural arrangement makes MFC flexible that can conform to a curved surface.

Due to the complexity of MFC materials, there are not many papers published dealing with modeling of MFC bonded smart structures for static and dynamic analysis. Nevertheless, some researchers simulated static response for MFC bonded smart structures using commercial software, e.g., ANSYS (Dano *et al*. 2008, Bowen *et al.*

*Corresponding author, Ph.D.
E-mail: zxwang@nwpu.edu.cn
[a] Ph.D.
E-mail: sqzhang@nwpu.edu.cn
[b] Ph.D.
E-mail: min.chen@xjtlu.edu.cn
[c] Ph.D.
E-mail: zhaogz@dlut.edu.cn
[d] Ph.D.
E-mail: schmidt@iam.rwth-aachen.de
[e] Ph.D.
E-mail: xsqin@nwpu.edu.cn

Copyright © 2017 Techno-Press, Ltd.
http://www.techno-press.com/journals/sss&subpage=8
ISSN: 1738-1584 (Print), 1738-1991 (Online)

2011), ABAQUS (Ren 2008, Binette *et al.* 2009), and obtained reasonable predictions compared with those from the experiments. Beyond using the commercial software, Park and Kim (2005), Bilgen *et al*. (2010) developed analytical models respectively for MFC bonded active twist rotor blades and benders. Zhang et al. (2015b) developed a finite element model for static analysis of MFC bonded structures with arbitrary piezo fiber orientation based on the first-order shear deformation hypothesis. Azzouz *et al.* (2001) developed linear finite element models for static analysis of MFC or AFC laminated structures. Concerning dynamic analysis, Bilgen *et al.* (2010) developed an analytical model for frequency response analysis of an MFC bonded clamped-free thin beam, and compared with experimental results. Padoin *et al.* (2015) optimized the placement of MFC patches on a plate for vibration suppression using linear quadratic regulator (LQR) approach. In addition, Gao and Shen (2003), Sodano *et al*. (2004), Kim *et al.* (2011) used MFC patches for the applications of active vibration suppression. Moreover, Azzouz and Hall (2010) developed a von Kármán nonlinear FE model based on the FOSD hypothesis for frequency response of a rotating MFC actuator.

Apart from fiber based piezoelectric materials, many other conventional monolithic piezoelectric materials, such as piezoelectric ceramics and polymers, have been frequently used for shape and vibration control. A lot of publications can be found for shape and vibration control of monolithic piezoelectric bonded smart structures. An early literature review on static and dynamic control of piezoelectric structures was carried out by Irschik (2002). Many investigations have been carried out by Nader et al. (2003), Irschik *et al*. (2003), Schoeftner and Irschik (2011) for dynamic shape control of flexible beam-type structures using Bernoulli-Euler or Timoshenko beam hypothesis. Furthermore, Kioua and Mirza (2000) studied the bending and twisting behavior of piezoelectric laminated composite shallow shells. Wang *et al.* (2016) optimized the actuation locations using annealing algorithm for static shape control of smart reflector. Recently, Zhang and Schmidt (2014a, b), Zhang *et al*. (2015a) developed geometrically nonlinear models for shape and dynamic control of piezolaminated smart plates and shells. The literature survey reveals that most of the studies concerning shape and vibration control were focusing on conventional monolithic piezoelectric integrated smart structures. Due to many highlighted advantages of macro-fiber composites, some researchers started to investigate the modeling and analysis of MFC bonded structures. However, most of the available studies on simulation of MFC bonded structures was carried out using commercial software or simplified analytical solutions only for static analysis of beams and plates, and did not take the fiber angle variation into account, which certainly will influence significantly the structural response. On the other hand, very few papers presented and compared the two modes of MFC patches, namely MFC-d31and MFC-33. In order to simulate shape and vibration control of MFC bonded structures, this paper develops linear electro-mechanically coupled static and dynamic FE models using 2-dimensional finite elements based on the FOSD hypothesis Two different types of MFCs are compared and discussed, namely MFCd31 and MFC-d33, in which the former one is dominated by the d_{31} effect, while the latter one is by the d_{33} effect. The proposed model is firstly validated by a cantilevered plate bonded with MFC-d33, then applied to analyze a plate laminated with one of these two different MFCs for active shape and vibration control.

2. MFC constitutive equations

Macro-fiber composites are mainly comprised of piezoceramic fibers, epoxy matrix, electrode layers etc., see Li *et al.* (2016). Due to the difference of piezo-fiber polarization in MFC patches, there are two typical modes of MFCs, namely MFC-d31 and MFC-d33, with the principle descriptions shown in Fig. 1. The former one is dominated by the d31 effect, while the latter one mainly uses the d33 effect. This is due to the fact that the polarization of piezoelectric fibers in MFC-d31 is along the thickness direction and that in MFC-d33 is along the in-plane fiber direction.

In order to show clearly the process of modeling techniques for MFCs, three coordinate systems are employed, namely the curvilinear coordinate system denoted by Θ^i (i = 1, 2, 3), the fiber coordinate system presented by $\breve{\Theta}^i$, and the polarization coordinate system shown as $\tilde{\breve{\Theta}}^i$, as can be seen in Fig. 1, more details are referred to Zhang *et al*. (2015b). The polarization of both types of MFCs is along the $\tilde{\breve{\Theta}}^3$ -line in the polarization coordinate system. The quantities referred to the curvilinear coordinate system and the fiber coordinate system are respectively denoted by without overhead symbol and with overhead.

Using the assumption of $\breve{\sigma}_{33} = 0$ for plate and shell structures, the constitutive equations in the fiber coordinate system can be arranged in matrix form as

$$\breve{\boldsymbol{\sigma}} = \breve{\boldsymbol{c}}\breve{\boldsymbol{\varepsilon}} - \breve{\boldsymbol{e}}^{\mathrm{T}}\breve{\boldsymbol{E}}, \tag{1}$$

$$\breve{\boldsymbol{D}} = \breve{\boldsymbol{e}}\breve{\boldsymbol{\varepsilon}} + \breve{\boldsymbol{\chi}}\breve{\boldsymbol{E}}. \tag{2}$$

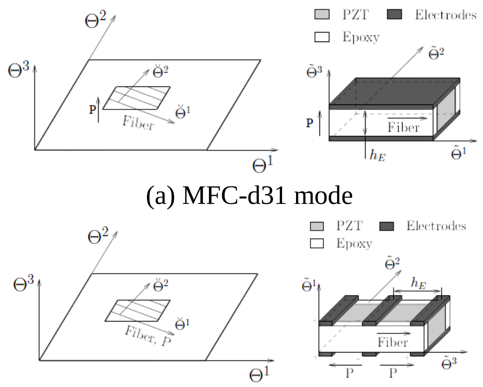

(a) MFC-d31 mode

(b) MFC-d33 mode

Fig. 1 Two typical modes of MFC

Here $\breve{\boldsymbol{\sigma}}$, $\breve{\boldsymbol{\varepsilon}}$ are the stress and strain vectors; $\breve{\boldsymbol{c}}$ is the elasticity constant matrix; $\breve{\boldsymbol{D}}$, $\breve{\boldsymbol{E}}$, $\breve{\boldsymbol{e}}$ and $\breve{\boldsymbol{\chi}}$ denote the electric displacement vector, the electric field vector, the piezoelectric constant matrix and the dielectric constant matrix, respectively.

Due to different polarization of MFC, the piezoelectric constant matrix has different forms for the two modes under consideration. For MFC-d31, the piezoelectric constant matrix is arranged as

$$\breve{\boldsymbol{e}} = \begin{bmatrix} 0 & 0 & 0 & 0 & \breve{e}_{15} \\ 0 & 0 & 0 & \breve{e}_{24} & 0 \\ \breve{e}_{31} & \breve{e}_{32} & 0 & 0 & 0 \end{bmatrix}, \tag{3}$$

while for MFC-d33, it becomes

$$\breve{\boldsymbol{e}} = \begin{bmatrix} \breve{e}_{11} & \breve{e}_{12} & 0 & 0 & 0 \\ 0 & 0 & 0 & \breve{e}_{26} & 0 \\ 0 & 0 & 0 & 0 & \breve{e}_{35} \end{bmatrix}. \tag{4}$$

Every piece of MFC patch, either MFC-d31 or MFC-d33, has only one direction in which the electric voltage is applied. Therefore, the constitutive equations for the direct piezoelectric effect of MFC material are reduced to

$$\breve{D}_p = \begin{bmatrix} \breve{e}_{p1} & \breve{e}_{p2} & 0 & 0 & 0 \end{bmatrix} \breve{\boldsymbol{\varepsilon}} + \breve{\chi}_{pp} \breve{E}_p. \tag{5}$$

The components in (5) can be obtained by

$$\breve{e}_{p1} = \breve{d}_{p1}\breve{c}_{11} + \breve{d}_{p2}\breve{c}_{12}, \tag{6}$$

$$\breve{e}_{p2} = \breve{d}_{p1}\breve{c}_{12} + \breve{d}_{p2}\breve{c}_{22}, \tag{7}$$

$$\breve{\chi}_{pp} = \breve{\epsilon}_{pp} - \breve{d}_{p1}\breve{e}_{p1} - \breve{d}_{p2}\breve{e}_{p2}, \tag{8}$$

$$\breve{E}_p = -\frac{\breve{\phi}_p}{h_{\mathrm{E}}}, \tag{9}$$

where p = 3 for MFC-d31 and p = 1 for MFC-d33, $\breve{d}_{ij}$ refer to the piezoelectric constants, $\breve{\epsilon}_{pp}$ represents the dielectric constants, $\breve{\phi}_p$ is the actuation voltage applied on two electrodes and h_E denotes the distance between two neighboring electrodes.

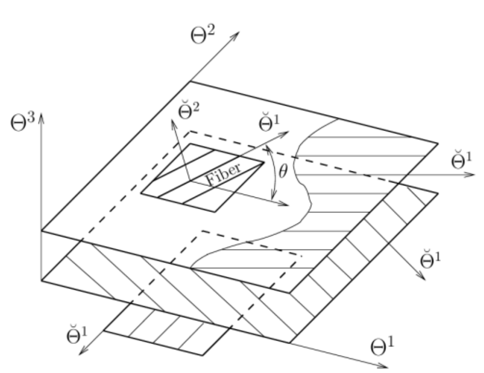

Fig. 2 Multi-layer composites with MFCs

Considering multi-layered structures laminated with MFC patches and cross- or angle-ply laminae, as illustrated in Fig. 2, one has to transform the constitutive equations in the fiber coordinate system to the curvilinear coordinate system by a transformation matrix $\boldsymbol{T}$, with the details presented in Zhang *et al.* (2015b). Consequently, the constitutive equations referred to the curvilinear coordinate system become

$$\boldsymbol{\sigma} = \boldsymbol{c}\varepsilon - \boldsymbol{e}^{\mathrm{T}}\boldsymbol{E}, \tag{10}$$

$$\boldsymbol{D} = e\boldsymbol{\varepsilon} + \boldsymbol{\chi}\boldsymbol{E}. \tag{11}$$

with

$$\boldsymbol{c} = \boldsymbol{T}^{\mathrm{T}}\breve{\boldsymbol{c}}\boldsymbol{T},\ \boldsymbol{e} = \breve{\boldsymbol{e}}\boldsymbol{T},\ \boldsymbol{\chi} = \breve{\boldsymbol{\chi}}. \tag{12}$$

From the structural arrangement of MFC-d31 and MFC-d33 patches, it can be known that the electric field applied on MFC is always along the thickness direction for MFC-d31 patches and along the piezo fiber direction for MFC-d33 patches. The electric field induced longitudinal strains ($\breve{\varepsilon}_{11}, \breve{\varepsilon}_{22}$) are respectively parallel to $\breve{\Theta}^1$ and $\breve{\Theta}^2$, which are transformed to structural coordinates by the matrix $\boldsymbol{T}$.

3. Dynamic finite element formulations

For laminated thin-walled structures, a 2-dimensional finite element with the FOSD hypothesis is adopted. Under the assumption of the FOSD hypothesis, the displacement through the thickness is regarded as linear distribution, more details are referred to Zhang et al. (2015b).

In order to obtain dynamic equations of motion, the Hamilton's principle is applied with taking into account the linear stain-displacement relations, given as

$$\int_{t_1}^{t_2} (\delta T - \delta W_{\mathrm{int}} + \delta W_{\mathrm{ext}}) \mathrm{d}t = 0, \tag{13}$$

with

$$\delta T = -\int_V \rho \delta \boldsymbol{u}^{\mathrm{T}} \ddot{\boldsymbol{u}} \mathrm{d}V, \tag{14}$$

$$\delta W_{\mathrm{int}} = \int_V (\delta \boldsymbol{\varepsilon}^{\mathrm{T}} \boldsymbol{\sigma} - \delta \boldsymbol{E}^{\mathrm{T}} \boldsymbol{D}) \mathrm{d}V, \tag{15}$$

$$\delta W_{\mathrm{ext}} = \int_V \delta \boldsymbol{u}^{\mathrm{T}} \boldsymbol{f}_{\mathrm{b}} \,\mathrm{d}V + \int_A \delta \boldsymbol{u}^{\mathrm{T}} \boldsymbol{f}_{\mathrm{s}} \,\mathrm{d}A + \delta \boldsymbol{u}^{\mathrm{T}} \boldsymbol{f}_{\mathrm{c}}. \tag{16}$$

Here δ represents the variational operator, $\int_A \cdot \mathrm{d}A$ is the area integral and $\int_V \cdot \mathrm{d}V$ denotes the volume integral; T, W_{int}, W_{ext} denote respectively the kinetic energy, internal work and the external work; $\boldsymbol{f}_{\mathrm{b}}$, $\boldsymbol{f}_{\mathrm{s}}$ and $\boldsymbol{f}_{\mathrm{c}}$ are the body, surface and concentrated force vectors, respectively, and $\boldsymbol{u}$, $\ddot{\boldsymbol{u}}$ are respectively the displacement and acceleration vectors.

Solving Eq. (13) one obtains the equations of motion and the sensor equations for MFC bonded composite structures as

$$\boldsymbol{M}_{\mathrm{uu}}\ddot{\boldsymbol{q}}+\boldsymbol{C}_{\mathrm{uu}}\dot{\boldsymbol{q}}+\boldsymbol{K}_{\mathrm{uu}}\boldsymbol{q}+\boldsymbol{K}_{\mathrm{u}\phi}\boldsymbol{\phi}_{\mathrm{a}}=\boldsymbol{F}_{\mathrm{ue}}, \tag{17}$$

$$\boldsymbol{K}_{\phi\mathrm{u}}\boldsymbol{q}+\boldsymbol{K}_{\phi\phi}\boldsymbol{\phi}_{\mathrm{s}}=\boldsymbol{0}. \tag{18}$$

Here $\boldsymbol{M}_{\mathrm{uu}}$, $\boldsymbol{C}_{\mathrm{uu}}$, $\boldsymbol{K}_{\mathrm{uu}}$, $\boldsymbol{K}_{\mathrm{u}\phi}$, $\boldsymbol{K}_{\phi\mathrm{u}}$ and $\boldsymbol{K}_{\phi\phi}$ represent the mass matrix, the damping matrix, the stiffness matrix, the piezoelectric coupled stiffness matrix, the mechanically coupled capacity matrix and the piezoelectric capacity matrix, respectively. Furthermore, $\boldsymbol{F}_{\mathrm{ue}}$, $\boldsymbol{q}$, $\boldsymbol{\phi}_{\mathrm{a}}$ and $\boldsymbol{\phi}_{\mathrm{s}}$ are respectively the external force vector, the nodal displacement vector, the actuation voltage vector and the sensor voltage vector. For static analysis the first two terms ($\boldsymbol{M}_{\mathrm{uu}}\ddot{\boldsymbol{q}}, \boldsymbol{C}_{\mathrm{uu}}\dot{\boldsymbol{q}}$) in Eq. (17) are neglected.

4. Optimized control

To implement an optimal control strategy, a state space model should be constructed. Assuming the state vector x, the system input vector $\boldsymbol{u}$ and output vector $\boldsymbol{y}$ as

$$\boldsymbol{x}=\begin{Bmatrix}\boldsymbol{q}\\ \dot{\boldsymbol{q}}\end{Bmatrix},\ \boldsymbol{u}=\boldsymbol{\phi}_{\mathrm{a}},\ \boldsymbol{y}=\boldsymbol{q}. \tag{19}$$

one obtains a standard form of the state space model as

$$\dot{\boldsymbol{x}}=\boldsymbol{A}\boldsymbol{x}+\boldsymbol{B}\boldsymbol{u}, \tag{20}$$

$$\boldsymbol{y}=\boldsymbol{C}\boldsymbol{x}. \tag{21}$$

Here the system matrix $\boldsymbol{A}$, the control matrix $\boldsymbol{B}$ and the system output matrix $\boldsymbol{C}$ are respectively expressed as

$$\boldsymbol{A}=\begin{bmatrix}\boldsymbol{0} & \boldsymbol{I}\\ -\boldsymbol{M}_{\mathrm{uu}}{}^{-1}\boldsymbol{K}_{\mathrm{uu}} & -\boldsymbol{M}_{\mathrm{uu}}{}^{-1}\boldsymbol{C}_{\mathrm{uu}}\end{bmatrix}, \tag{22}$$

$$\boldsymbol{B}=\begin{bmatrix}\boldsymbol{0}\\ -\boldsymbol{M}_{\mathrm{uu}}{}^{-1}\boldsymbol{K}_{\mathrm{u}\phi}\end{bmatrix}, \tag{23}$$

$$\boldsymbol{C}=\begin{bmatrix}\boldsymbol{I} & \boldsymbol{0}\end{bmatrix}, \tag{24}$$

where $\boldsymbol{I}$ and $\boldsymbol{0}$ denote respectively the identity matrix and zero matrix.

Linear quadratic regulator (LQR) is proposed for vibration suppression in the present paper. The control gain then can be obtained by optimizing the cost function

$$J_{\mathrm{LQR}}=\int_0^{\infty}(\boldsymbol{y}^{\mathrm{T}}\bar{\boldsymbol{Q}}\boldsymbol{y}+\boldsymbol{u}^{\mathrm{T}}\bar{\boldsymbol{R}}\boldsymbol{u})\mathrm{d}t, \tag{25}$$

where $\bar{Q}$ and $\bar{R}$ are the weighting matrices for the system output and the system input vectors. The optimized control input will be

$$\boldsymbol{u}=-\boldsymbol{K}\boldsymbol{x}=-\bar{\boldsymbol{R}}^{-1}\boldsymbol{B}^{\mathrm{T}}\boldsymbol{P}\boldsymbol{x}. \tag{26}$$

Here $\boldsymbol{K}=\bar{\boldsymbol{R}}^{-1}\boldsymbol{B}^{\mathrm{T}}\boldsymbol{P}$ is the control gain, and $\boldsymbol{P}$ can be solved by the algebraic Riccati equation, more details are referred to Zhang *et al.* (2015c).

5. Numerical simulations

5.1 Validation test

In order to validate the present finite element model, a cantilevered composite laminated plate bonded with an MFC actuation is tested numerically, which was studied earlier by Dano *et al.* (2008) and Padoin *et al.* (2015). The schematic drawing of the MFC composite plate is shown in Fig. 3, in which the dimensions of the host composite plate is 250×100×0.33 mm^3 and those of the active area of MFC patch is 85×28×0.3 mm^3. In the simulation only the active area is considered of both cases of MFCs, because the non-active area is made up of kapton material that is negligible soft (Zhang *et al*. 2016). The host composite structure is made up of two plies stacked as $[0]_{\mathrm{s}}$, with the thickness of 0.165 mm for each substrate layer. The MFC patches simulated in the present paper is marked by M8528-P1/F1 for MFC-d33 mode and by M8528-P2 for MFC-d31 mode (Smart Material Corp. 2016). The spacing of the interdigitated electrodes is h_{E}=0.5 mm for M8528-P1/F1 and h_{E} = 0.18 mm for M8528-P2. The material properties of the composite layers and MFC patches are listed in Table 1.

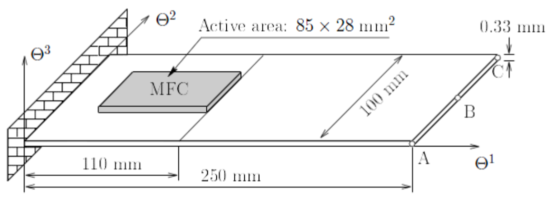

Fig. 3 Cantilevered composite laminated plate with a bonded MFC actuation active

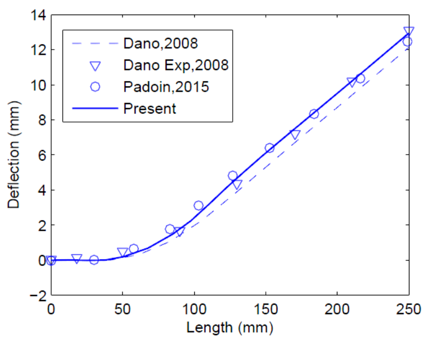

Fig. 4 Vertical displacements of the central line at the MFC plate with piezoelectric fiber angle 0° subjected to 1000 V actuation

Table 1 Material properties of MFCs and composites (Dano *et al*. 2008, Padoin *et al*. 2015, Smart Material Corp. 2016)

Material constants	MFC-d33	MFC-d31	Composite
$\breve{Y}_1$ (GPa)	30.336	30.336	101.6
$\breve{Y}_2$ (GPa)	15.857	15.857	7.91
$\breve{Y}_3$ (GPa)	15.857	15.857	7.91
$\breve{G}_{12}$ (GPa)	5.515	5.515	3.01
$\breve{G}_{13}$ (GPa)	5.515	5.515	3.01
$\breve{G}_{23}$ (GPa)	2.6	2.6	2.71
$\breve{v}_{12}$	0.312	0.312	0.318
$\breve{v}_{13}$	0.312	0.312	0.318
$\breve{v}_{23}$	0.327	0.327	0.458
$\breve{d}_{p1}$ (10^{-12}m/V)*	360	-129.6	
$\breve{d}_{p2}$ (10^{-12}m/V)*	-190	-68.4	
h_E (mm)	0.5	0.18	

The MFC bonded structure is meshed by 10×6 eight-node quadrilateral elements with five mechanical degrees of freedom at each node and one electrical degree of freedom on each MFC patch. Using the present finite element model, a static response of the central line at the cantilevered MFC plate subjected to 1000V actuation voltages is obtained and shown in Fig. 4. The results show that the present curve agrees quite well with those studied numerically by Padoin *et al*. (2015) and experimentally by Dano *et al*. (2008). However, a slight discrepancy exists when compared to the simulation result of Dano *et al.* (2008).

5.2 Static analysis of MFC bonded plate

In this subsection, the same MFC composite plate, shown in Fig. 3, is considered for static simulation. The plate is bonded with one MFC patch, either M8528-P1 (MFC-d33) or M8528-P2 (MFC-d31), which is subjected to an electric voltage of 300 V for both types. Since the distance of any two neighboring electrodes of MFC-d31 is different from those of MFC-d33, the electric field along the thickness for MFC-d31 and that along the piezo fiber orientation for MFC-d33 are respectively 300/0.18 V/mm and 300/0.5 V/mm. The vertical displacements at the central line for both cases are presented in Fig. 5, where the piezo fiber angle is zero. The figure shows that the central line displacements of two different MFCs are quite similar with a slight discrepancy. This is because the absolute value of the electric field induced longitudinal strain in the Θ^1 direction for MFC-d33 ($\varepsilon_{11} = |d_{11}E_1| = 2.16\times10^{-4}$) is equal to that for MFC-d31, as well as for the strain in the Θ^2 direction $\varepsilon_{22} = |d_{12}E_1| = 1.14\times10^{-4}$ in both types of MFCs. The slight discrepancy of the central line displacement is due to the sign of the piezoelectric coefficients.

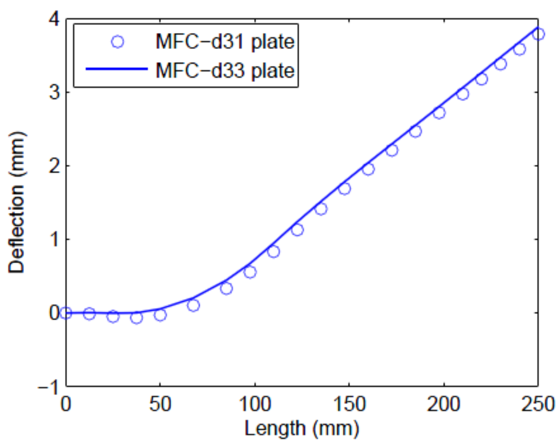

Fig. 5 Vertical displacements of the central line at the MFC plate with piezoelectric fiber angle 0° subjected to 300 V actuation voltage

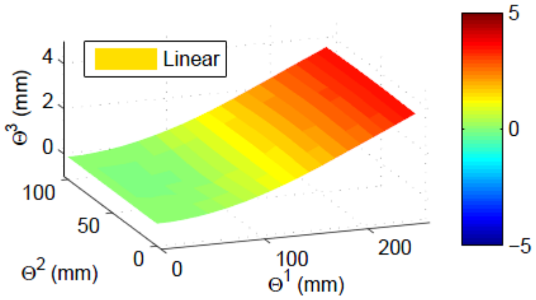

(a) MFC-d31 bonded plate

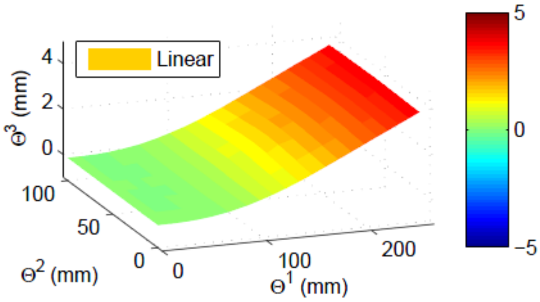

(b) MFC-d33 bonded plate

Fig. 6 Surface shapes of the composite plate with MFC piezoelectric fiber angle 0°

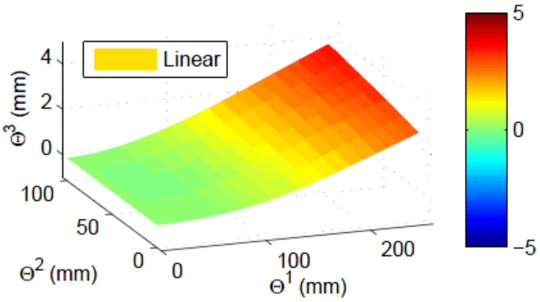

(a) MFC-d31 bonded plate

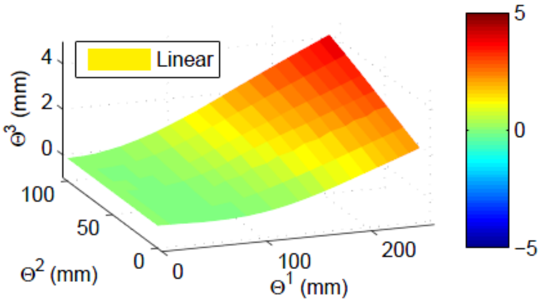

(b) MFC-d33 bonded plate

Fig. 7 Surface shapes of the composite plate with MFC piezoelectric fiber angle 15°

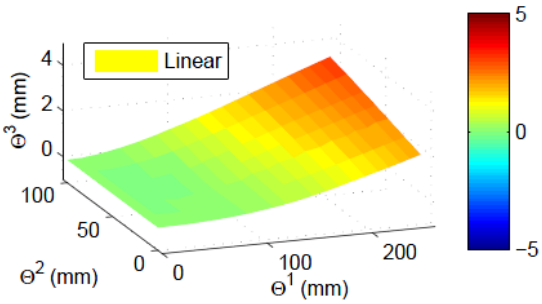

(a) MFC-d31 bonded plate

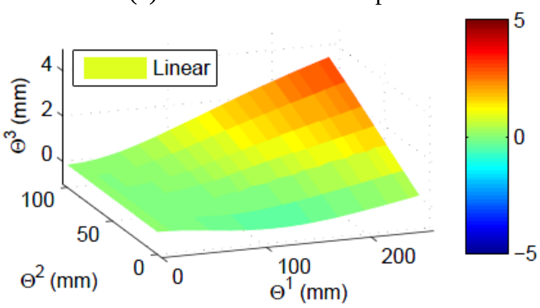

(b) MFC-d33 bonded plate

Fig. 8 Surface shapes of the composite plate with MFC piezoelectric fiber angle 30°

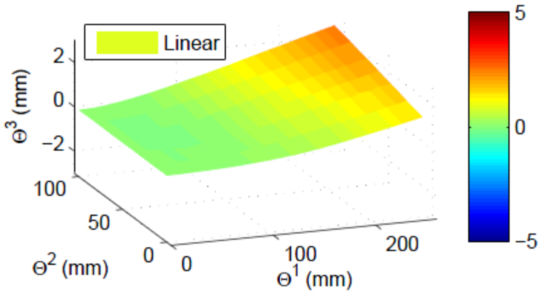

(a) MFC-d31 bonded plate

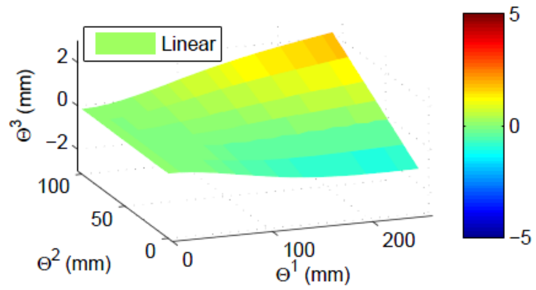

(b) MFC-d33 bonded plate

Fig. 9 Surface shapes of the composite plate with MFC piezoelectric fiber angle 45°

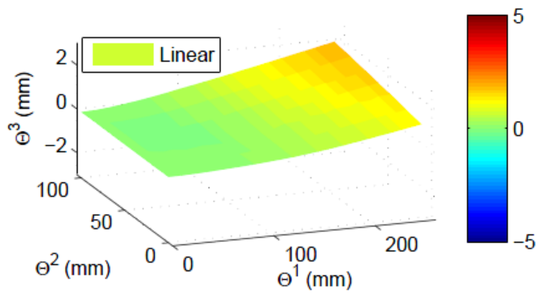

(a) MFC-d31 bonded plate

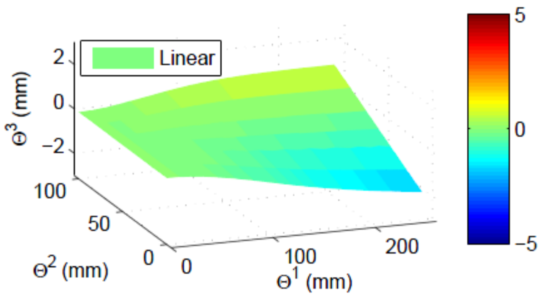

(b) MFC-d33 bonded plate

Fig. 10 Surface shapes of the composite plate with MFC piezoelectric fiber angle 60°

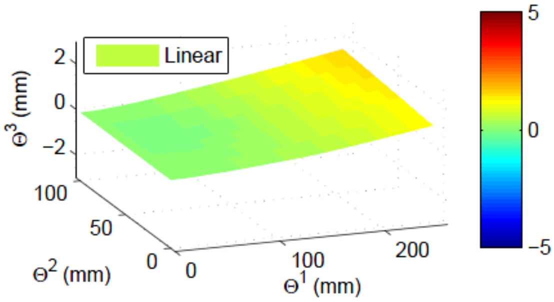

(a) MFC-d31 bonded plate

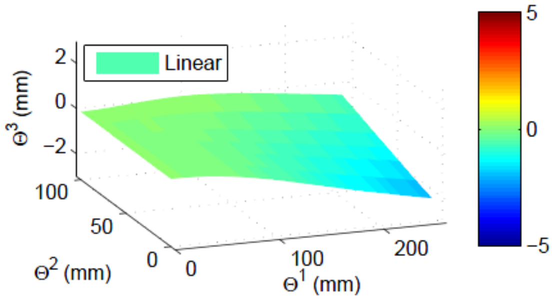

(b) MFC-d33 bonded plate

Fig. 11 Surface shapes of the composite plate with MFC piezoelectric fiber angle 75°

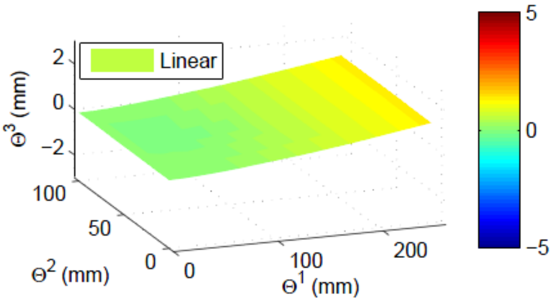

(a) MFC-d31 bonded plate

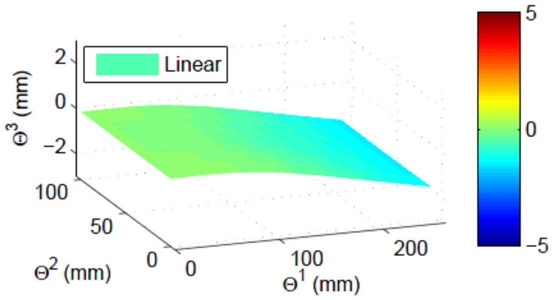

(b) MFC-d33 bonded plate

Fig. 12 Surface shapes of the composite plate with MFC piezoelectric fiber angle 90°

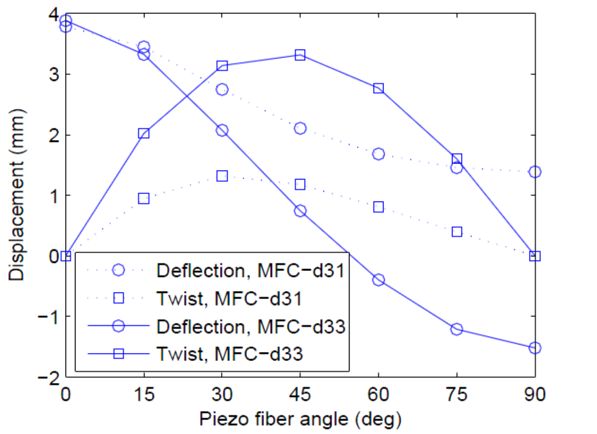

Fig. 13 Vertical deflections and twists of the MFC bonded composite plate

Considering the same boundary conditions, the deformed shapes of the laminated plate with various piezoelectric fiber orientations are presented in Figs. 6-12. From Fig. 6, it can be seen that the deformation is similar for either MFC-d31 or MFC-d33 bonded plates, in which the reason is explained in the previous paragraph. Since the piezoelectric constants of MFC-d31, $\breve{d}_{31}$ and $\breve{d}_{32}$, are in the same sign, MFC-d31 plate is always deformed in one direction, upwards or downwards. However, this will be changed in MFC-d33 plate. Because the piezoelectric constants of MFC-d33, $\breve{d}_{11}$ and $\breve{d}_{12}$, have opposite signs. The figures show that the MFC-d33 plate first deforms upwards, and then goes downwards with increasing of the piezoelectric fiber orientation form 0° to 90°. This can be explained by the fact that the deformation of the plate first is dominated by $\breve{d}_{11}$ constant (positive), and then dominated by $\breve{d}_{12}$ constant (negative), which has opposite sign. Furthermore, the plate bonded with MFC-d33 patch has much larger twists than that bonded with MFC-d31 patch, especially when the piezo fiber orientation placed at 30°, 45° and 60°. The vertical tip displacements w_B of the composite plate with various piezo fiber angles are presented in Fig. 13, as well as the twists defined as $|w_A - w_C|$.

5.3 Dynamic analysis and active vibration control

In this simulation, a step actuation voltage of 300 V is applied on the MFC patch, considering different types of MFC patches and various piezoelectric fiber orientations. The dynamic finite element model takes the consideration of damping effects, which are approximately obtained by the Rayleigh method with a damping ratio of 0.8% for the first six modes. The dynamic step response of the plate is presented in Fig. 14, from which we can observe that the dynamic response of MFC-d33 and MFC-d31 bonded plate with piezo fiber angle of 0° is almost identical. The amplitudes of dynamic response of the MFC bonded plate decreases dramatically with the piezo fiber angle increases, especially for the d33 mode. This trend can be concluded from static analysis in the previous subsection.

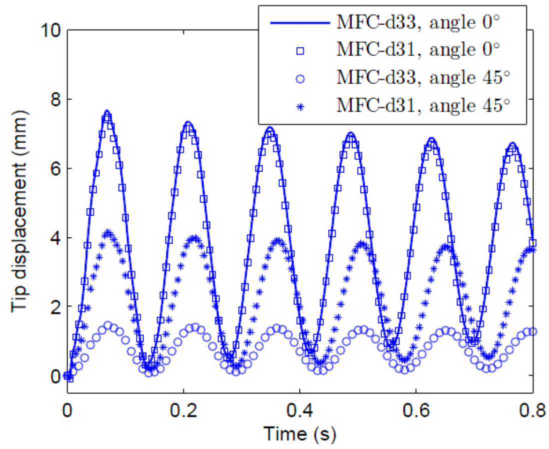

Fig. 14 Tip displacement of the MFC structures with various piezoelectric fiber orientation subjected to a step actuation voltage of 300 V

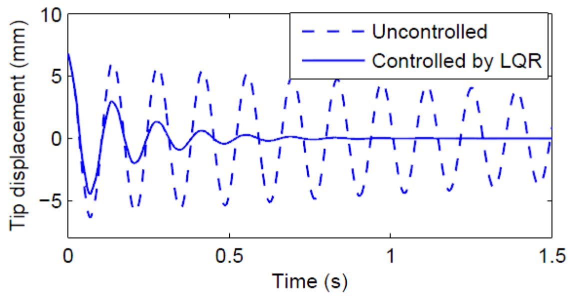

(a) Tip displacement

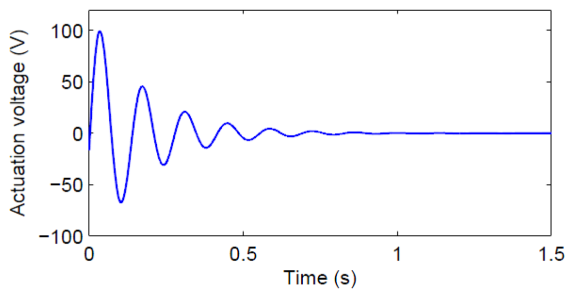

(b) Actuation voltage

Fig. 15 Active vibration control for the plate with MFC piezoelectric fiber angle 0° using LQR

Next, an LQR controller is adopted to suppress the free vibration of the MFC-d33 bonded composite plate with piezo fiber angle 0°. The plate is initially subjected to a concentrating tip force of 0.05 N, and the plate starts free vibration after the tip force is released. The weighting coefficients for the output and input are respectively $\bar{Q}$ =1/25 and $\bar{R}$ =10^{-4}. The controlled/uncontrolled free vibration and the actuation voltage are presented in Fig. 15, which shows that the free vibration is damped significantly by LQR controller. With the same structure and parameters, the frequency response of uncontrolled and controlled by LQR is obtained, shown in Fig. 16. From the frequency-magnitude plot, it can be seen that the first resonance frequency is well suppressed by the LQR controller.

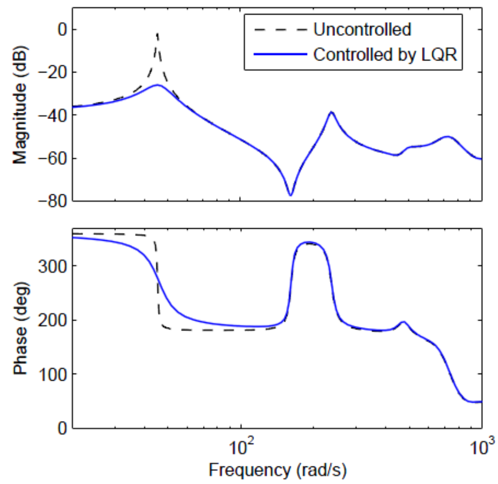

Fig. 16 Bode plot of the MFC-d33 structure with and without control

6. Conclusions

The paper has developed an electro-mechanically coupled dynamic FE model of MFC laminated structures for active shape and vibration control. The FE model is obtained by a 2-dimensional FE method based on the first-order shear deformation hypothesis. Two different types of MFCs (MFC-d31 and MFC-d33) have been considered in the present mathematical model. A composite plate bonded with either MFC-d31 or MFC-d33 has been studied for active shape and vibration control. The static results show that the piezoelectric fiber orientation has a significant influence on tip displacements and the twists both for MFC-d31 and MFC-d33 cases. With the equivalent piezoelectric constants (generating equal longitudinal strains), MFC-d33 bonded composite plate produces larger twists than MFCd31. Furthermore, the piezoelectric fiber orientation influences much more significantly in the MFC-d33 bonded plate than in MFC-d31 bonded plate.

Acknowledgements

This work was carried out with the support from the National Natural Science Foundation of China (Grant Nos. 11602193, 51505380), the Opening Fund of State Key Laboratory of Structural Analysis for Industrial Equipment, Dalian University of Technology, China (Grant No. GZ15212), University Natural Science Research Programme of Jiangsu Province, China, (Grant No. 16KJB460021), and the "111 project" of China (Grant No. B13044).

References

Azzouz, M.S., Mei, C. Bevan, J.S. and Ro, J.J. (2001), "Finite element modeling of MFC/AFC actuators and performance of MFC", *J. Intell. Mat. Syst. Str.*, **12**, 601-612.

Azzouz, M.S. and Hall, C. (2010), "Nonlinear finite element analysis of a rotating MFC actuator", *Proceedings of the 51st*

AIAA/ASME/ASCE/AHS/ASC Structures, Structural Dynamics, and Materials Conference, Orlando, Florida, April.

Bent, A.A. and Hagood, N.W. (1997), "Piezoelectric fiber composite with integrated electrodes", *J. Intel. Mat. Syst. Str.*, **8**, 903-919.

Bilgen, O., Erturk, A. and Inman, D.J. (2010), "Analytical and experimental characterization of macrofibercomposite actuated thin clamped-free unimorph benders", *J. Vib. Acoust.*, **132**(5), 051005.

Binette, P., Dano, M.L. and Gendron, G. (2009), "Active shape control of composite structures under thermal loading", *Smart Mater. Struct.*, **18**, 025007.

Bowen, C.R., Giddings, P.F., Salo, A.I.T. and Kim, H.A. (2011), "Modeling and characterization of piezoelectrically actuated bistable composites", *IEEE T. Ultrason. Ferr.*, **58**(9), 1737-1750.

Dano, M.L., Gakwaya, M. and Julliere, B. (2008), "Compensation of thermally induced distortion in composites structures using macro-fiber composites", *J. Intel. Mat. Syst. Str.*, **19**, 225-233.

Gao, J.X. and Shen, Y.P. (2003), "Active control of geometrically nonlinear transient vibration of composite plates with piezoelectric actuators", *J. Sound Vib.*, **264**(4), 911-928.

Hagood, N., Kindel, R., Ghandi, K. and Gaudenzi, P. (1993), "Improving transverse actuation of piezoceramics using interdigitated surface electrodes", *Proceedings of the SPIE - Smart Structures and Materials 1993: Smart Structures and Intelligent Systems*, SPIE: **1917**, 341–352, Albuquerque, New Mexico.

Irschik, H. (2002), "A review on static and dynamic shape control of structures by piezoelectric actuation", *Eng. Struct.*, **24**, 5-11.

Irschik, H., Krommer, M. and Pichler, U. (2003), "Dynamic shape control of beam-type structures by piezoelectric actuation and sensing", *Int. J. Appl. Electromag. Mech.*, **17**, 251-258.

Kim, H.S., Sohn, J.W. and Choi, S.B. (2011), "Vibration control of a cylindrical shell structure using macro fiber composite actuators", *Mech. Based Des. Struc.*, **39**, 491-506.

Kioua, H. and Mirza, S. (2000), "Piezoelectric induced bending and twisting of laminated composite shallow shells", *Smart Mate. Struct.*, **9**, 476-484.

Konka, H.P., Wahab, M.A. and Lian, K. (2013), "Piezoelectric fiber composite transducers for health monitoring in composite structures", *Sensor. Actuat. A - Phys.*, **194**, 84-94.

Li, Y.X., Zhang, S.Q., Schmidt, R. and Qin, X.S. (2016), "Homogenization for macro-fiber composites using reissner-mindlin plate theory", *J. Intel. Mat. Syst. Str.*, **27**(18), 2477-2488.

Lin, X.J., Zhou, K.C., Zhang, X.Y. and Zhang, D. (2013), "Development, modeling and application of piezoelectric fiber composites", *T. Nonferrous Metals Soc. China*, **23**, 98-107.

Nader, M., Gattringer, H., Krommer, M. and Irschik, H. (2003), "Shape control of flexural vibrations of circular plates by shaped piezoelectric actuation", *J. Vib. Acoust.*, **125**(1), 88-94.

Padoin, E., Fonseca, J.S.O., Perondi, E.A. and Menuzzi, O. (2015), "Optimal placement of piezoelectric macro fiber composite patches on composite plates for vibration suppression", *Latin Am. J. Solids Struct.*, **12**(5), 925-947.

Park, J.S. and Kim, J.H. (2005), "Analytical development of single crystal macro fiber composite actuators for active twist rotor blades", *Smart Mater. Struct.*, **14**, 745-753.

Ren, L. (2008), "A theoretical study on shape control of arbitrary lay-up laminates using piezoelectric actuators", *Compos. Struct.*, **83**, 110-118.

Schoeftner, J. and Irschik, H. (2011), "A comparative study of smart passive piezoelectric structures interacting with electric networks: Timoshenko beam theory versus finite element plane stress calculations", *Smart Mater. Struct.*, **20**, 025007.

Skinner, D.P., Newnham, R.E. and Cross, L.J.E. (1978), "Flexible composite transducers", *Mater. Res. Bull.*, **13**(6), 599-607.

Smart Material Corp (2016), *http://www.smart-material.com*.

Sodano, H.A., Park, G. and Inman, D.J. (2004), "An investigation into the performance of macro-fiber composites for sensing and structural vibration applications", *Mech. Syst. Signal Pr.*, **18**(3), 683-697.

Song, H.J., Choi, Y.T., Wereley, N.M. and Purekar, A.S. (2010), "Energy harvesting devices using macro-fiber composite materials", *J. Intel. Mat. Syst. Struct.*, **21**, 647-658.

Wang, Z., Cao, Y., Zhao, Y. and Wang, Z. (2016), "Modeling and optimal design for static shape control of smart reflector using simulated annealing algorithm", *J. Intel. Mat. Syst. Str.*, **27**(5), 705-720.

Wilkie, W.K., Bryant, R.G., High, J.W., Fox, R.L., Hellbaum, R.F., Jalink, A., Little, B.D. and Mirick, P.H. (2000), "Low-cost piezocomposite actuator for structural control applications", *SPIE - Smart Structures and Materials 2000: Industrial and Commercial Applications of Smart Structures Technologies*, **3991**, 323-334.

Williams, R.B., Grimsley, B.W., Inman, D.J. and Wilkie, W.K. (2002a), "Manufacturing and mechanics-based characterization of macro fiber composite actuators", *Proceedings of the ASME 2002 International Mechanical Engineering Congress and Exposition*. New Orleans, Louisiana, USA, November.

Williams, R.B., Wilkie, W.K. and Inman, D.J. (2002b), "An overview of composite actuators with piezoceramic fibers", *Proceedings of the IMAC-XX: Conference & Exposition on Structural Dynamics*, 4753, 421-427. Los Angeles, CA, USA.

Zhang, S.Q., Li, Y.X. and Schmidt, R. (2015a), "Active shape and vibration control for piezoelectric bonded composite structures using various geometric nonlinearities", *Compos. Struct.*, **122**, 239-249.

Zhang, S.Q., Li, Y.X. and Schmidt, R. (2015b), "Modeling and simulation of macro-fiber composite layered smart structures", *Compos. Struct.*, **126**, 89-100.

Zhang. S.Q. and Schmidt. R. (2014a), "Large rotation theory for static analysis of composite and piezoelectric laminated thin-walled structures", *Thin Wall. Struct.*, **78,** 16-25.

Zhang, S.Q. and Schmidt, R. (2014b), "Static and dynamic FE analysis of piezoelectric integrated thin-walled composite structures with large rotations", *Compos. Struct.*, **112**, 345-357.

Zhang, S.Q., Schmidt, R., Müller, P.C. and Qin, X.S. (2015c), "Disturbance rejection control for vibration suppression of smart beams and plates under a high frequency excitation", *J. Sound Vib.*, **353**, 19-37.

Zhang, S.Q., Wang, Z.X., Qin, X.S., Zhao, G.Z. and Schmidt, R. (2016), "Geometrically nonlinear analysis of composite laminated structures with multiple macro-fiber composite (MFC) actuators", *Compos. Struct.*, **150**, 62-72.

FC